The effect of temporal impulse response on experimental reduction of photon scatter in time-resolved diffuse optical tomography

2013 Phys. Med. Biol. 58 335

(http://iopscience.iop.org/0031-9155/58/2/335)

IOP Publishing Physics in Medicine and Biology

Phys. Med. Biol. **58** (2013) 335–349 doi:10.1088/0031-9155/58/2/335

The effect of temporal impulse response on experimental reduction of photon scatter in time-resolved diffuse optical tomography

Niksa Valim, James Brock, Miriam Leeser and Mark Niedre

Department of Electrical and Computer Engineering, Northeastern University, Boston, MA, 02115, USA

E-mail: mniedre@ece.neu.edu

Received 3 August 2012, in final form 30 October 2012
Published 21 December 2012
Online at stacks.iop.org/PMB/58/335

Abstract

New fast detector technology has driven significant renewed interest in time-resolved measurement of early photons in improving imaging resolution in diffuse optical tomography and fluorescence mediated tomography in recent years. In practice, selection of early photons results in significantly narrower instrument photon density sensitivity functions (PDSFs) than the continuous wave case, resulting in a better conditioned reconstruction problem. In this work, we studied the quantitative impact of the instrument temporal impulse response function (TIRF) on experimental PDSFs in tissue mimicking optical phantoms. We used a multimode fiber dispersion method to vary the system TIRF over a range of representative literature values. Substantial disagreement in PDSF width—by up to 40%—was observed between experimental measurements and Monte Carlo (MC) models of photon propagation over the range of TIRFs studied. On average, PDSFs were broadened by about 0.3 mm at the center plane of the 2 cm wide imaging chamber per 100 ps of the instrument TIRF at early times. Further, this broadening was comparable on both the source and detector sides. Results were confirmed by convolution of instrument TIRFs with MC simulations. These data also underscore the importance of correcting imaging PDSFs for the instrument TIRF when performing tomographic image reconstruction to ensure accurate data–model agreement.

(Some figures may appear in colour only in the online journal)

[1] Author to whom any correspondence should be addressed.

1. Introduction

Diffuse optical tomography (DOT) and fluorescence mediated tomography (FMT) are in increasing use as clinical and pre-clinical imaging modalities, wherein three-dimensional images of native tissue contrast, exogenous fluorescent markers or fluorescent proteins are reconstructed (Arridge 1999, Ntziachristos *et al* 2000, 2003, 2005, Boas *et al* 2001, Graves *et al* 2003). DOT and FMT instrumentation require measurement of photons that propagate through bulk biological tissue in the diffusive regime either in transmittance or reflectance modes (Culver *et al* 2003, Hielscher 2005). Images are obtained by relating measurements to the unknown quantity of interest (i.e. tissue optical properties or fluorescence concentrations) with physical models of light propagation in a system of linear equations, and then solution of the subsequent ill-posed inverse problem (Klose *et al* 2005). The most important technical limitation of both DOT and FMT is arguably the relatively low imaging resolution due to the high degree of light scatter in biological tissue, which is generally understood to be about 10–20% of the imaging length (Wang and Wu 2007). One well established approach to improve imaging resolution is time-resolved (TR) detection of 'early-arriving' or 'weakly-diffuse' photons. Photons that arrive on the rising edge of the transmitted intensity curve from a pulsed laser source have undergone significantly fewer total scattering events than the bulk photon population (i.e. time-integrated photons). As such, the width of the imaging photon density sensitivity function (PDSF; alternatively referred to as the 'weight function', 'photon measurement density function', Jacobian, or 'banana function') is correspondingly reduced, leading to a better conditioned image reconstruction problem and improved imaging resolution. Early work by Feld *et al* (Wu *et al* 1997) demonstrated this in localizing fluorescent inclusions with a fiber-coupled streak camera in bulk diffusive media, and the approach was studied by other groups in trans-illumination imaging geometries (Andersson-Engels *et al* 1990, Gandjbakhche *et al* 1994, Grosenick *et al* 1999). In recent years, there has been substantial renewed interest in the concept with the development of new classes of fast time-gated and TR detectors (Turner *et al* 2005, Leblond *et al* 2009, Niedre and Ntziachristos 2010, Valim *et al* 2010, Venugopal *et al* 2010b, Zhang *et al* 2011, Tosi *et al* 2011, LaPointe *et al* 2012).

Recently, we experimentally measured time-dependent PDSFs for a particular pulsed light source (super-continuum laser) and detector (fast photomultiplier tube (PMT)) combination (Valim *et al* 2010). Very briefly, we demonstrated substantial disagreement with experimentally measured PDSFs and theoretical results computed with TR Monte Carlo (MC) simulations, particularly at very early arrival times, i.e. earlier than the 10%-of-maximum point on the rising edge of the curve. At the time, we hypothesized that this effect was chiefly due to the finite (non-ideal) temporal impulse response function (TIRF) of our system, which was 163 ps. Although we did not confirm this explicitly, it is generally understood that 'faster is better' in the TR tomography literature. For example, other authors have shown that non-ideal instrument TIRFs can yield incorrect estimation of tissue optical properties from full time curves (Ntziachristos and Chance 2001, Liebert *et al* 2003), or can introduce of imaging artifacts when performing TR imaging with mean, variance, and 'skew' TR data-types (Hillman *et al* 2000). Other authors have similarly shown that this can lead to erroneous estimation of fluorescence lifetimes in TR FMT (Luchowski *et al* 2009, Gerega *et al* 2011).

However, to our knowledge the quantitative effects of the instrument TIRF on measurements in the early-photon regime have never been studied in detail previously. Of particular interest is the degree of experimental resolution improvement obtainable relative to the theoretical maximum. A survey of the literature published in TR DOT and FMT shows that previously reported TR instrument configurations have intrinsic system TIRFs in the range of approximately 80–800 ps. Multichannel plate (MCP)-based systems have reported TIRFs in

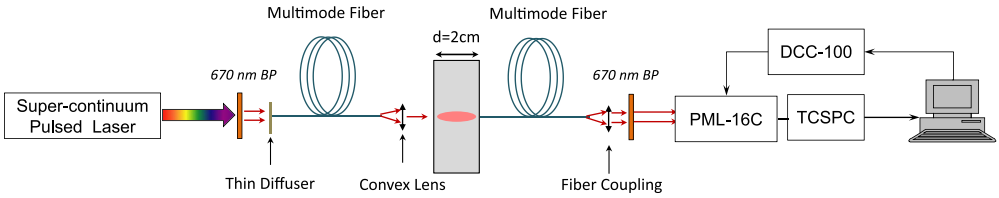

Figure 1. Schematic of the instrument used to measure system PDSFs. Two multimode optical fibers of varying lengths were coupled at the system input and output to alter the instrument TIRF.

the range of 80–200 ps (Andersson-Engels *et al* 1990, Pifferi *et al* 2004), PMT-based systems in the range of 160–800 ps (Grosenick *et al* 2003, Liebert *et al* 2004, Contini *et al* 2006, Kepshire *et al* 2009, Wabnitz *et al* 2010, Kacprzak *et al* 2012), intensified charge-coupled device camera (ICCD)-based systems in the range of 200–400 ps (Niedre *et al* 2006, Kumar *et al* 2008, Venugopal *et al* 2010a, Sawosz *et al* 2010, Zhao *et al* 2011), streak camera-based systems in the range of 150–250 ps (Wu *et al* 1997). Fast avalanche photodiode (APD) systems have recently been used in TR tomography with stated detector response time of about 40 ps (Bérubé-Lauzière and Robichaud 2007, Tosi *et al* 2011), although the overall system TIRF was not stated. Interferometric (i.e. transmission geometry optical coherence tomography) approaches have also been used to measure TR curves through diffusive media, but to date these have been limited to relatively small (∼1–5 mm) imaging volumes (Hee *et al* 1993, Li and Wang 2007).

In this work we quantitatively studied the impact of the instrument TIRF on imaging resolution by systematically modulating our instrument TIRF in approximately the range of reported literature values (specifically, between 163 and 716 ps) using a fiber dispersion method similar to previous authors (Ntziachristos *et al* 1998, Liebert *et al* 2003) and measured the impact of this on experimentally measured PDSFs. As we demonstrate, *all* instrument TIRFs that we tested resulted in significant disagreement (up to 40%) in PDSF width compared to TR MC theory. Experimental disagreement was most pronounced at very early time points (for example, at the 10%-of-peak point on the rising edge of the curve or earlier), and varied by about 0.3 mm per 100 ps of the instrument TIRF in this regime. We found that modulation of the system TIRF by elongating the response on either the source or detector side had comparable effects, implying that use of fast sources or detectors will yield approximately the same improvement in imaging resolution in a TR optical tomography system. This was also confirmed by temporal convolution of system TIRFs with the output of TR MC simulations. Effects of detector sensitivity and noise properties—which are also known to affect imaging resolution in DOT and FMT—were not studied here. The results presented here have significant implications, (i) in correct calculation of imaging PDSFs for TR DOT and FMT, and (ii) in design of TR DOT and FMT systems that utilize the early-photon effect.

2. Methods and materials

2.1. Instrumentation

The basic system used for these experiments is shown in figure 1 and is similar to the system we described previously (Valim *et al* 2010). A fast, pulsed super-continuum fiber laser with an 80 MHz repetition rate was used as the light source (KoherasSuper-K Power, NKT Photonics, Birkerod, Denmark). The output of the laser was passed through a 670 nm bandpass interference filter (30 nm full width at half maximum (FWHM); Chroma Technology, Bellows

Falls, VT). As we discussed previously (Valim *et al* 2010), the original broadband light pulse from the super-continuum source was approximately 400 ps FWHM, but after wavelength filtering was reduced to about 30 ps. Light was coupled into a 0.37 NA, 600 μm core step-index multimode optical fiber (BFL37-600; Thorlabs) of varying length by illuminating a diffusing glass plate (220-Grit ground glass diffuser, Edmund Optics, Barrington, NJ) placed directly in front of the fiber end (see section 2.2 below). Light exiting the fiber was focused to a 1 mm diameter spot on the surface of a custom made 15 cm $\times$ 15 cm $\times$ 2 cm glass sample chamber with a pair of plano-convex lenses (Edmund Optics). The thickness of the glass walls was about 2 mm. Neutral density (ND) filters were placed in the beam path so that the illumination intensity at the chamber surface was 1.25 mW. The sample chamber was filled with liquid phantoms prepared from a stock solution of 10% Intralipid (Baxter Healthcare Corporation, Deerfield, IL) and India ink. These were diluted so that the final liquid optical properties at 670 nm were approximately as follows: reduced scattering coefficient $\mu\prime_s = 10$ cm^{-1} and absorption coefficient $\mu_a = 0.15$ cm^{-1}. Here, the optical properties were estimated based on characterization of liquid phantom optical properties by TR analysis of transmitted intensity curves performed previously in Niedre *et al* (2006). Moreover, these optical properties were selected since they are approximately equivalent to typical literature values for biological tissue at red and near-infrared wavelengths (Tromberg *et al* 1997, Torricelli *et al* 2001, Niedre *et al* 2006).

Light transmitted through the 2 cm wide chamber was collected with a second multimode optical fiber that was placed co-axially with the position of the input beam. Given the 0.37 NA of the fiber and the 2 mm thickness of the chamber glass, the detection spot size on the inner surface of the chamber was about 1.5 mm. Light exiting the detector optical fiber was collimated using a SMA-coupled achromatic plano-convex lens package (F260 SMA-B; Thorlabs) and then passed through a second 670 nm bandpass filter (Chroma). The transmitted light was measured with a 16-channel PMT array (PML-16-C, Becker and Hickl, Berlin, Germany). The gain on the multi-anode PMT was controlled with a detector control card (DCC; Becker and Hickl) that was operated at 90% of maximum. The output of the PMT array was amplified with internal preamplifiers and coupled into a time-correlated single photon counting card (SPC-130, Becker and Hickl) configured so that it had a 16.3 ps temporal resolution. Although the PMT array had 16 individual anodes, it was determined that the detected light illuminated approximately the middle 6 detection channels. Therefore, the time-correlated photon count signals from only the middle 6 channels were summed after correction of the minor inter-channel time skew (<25 ps in this case). The overall system TIRF FWHM was measured to be 154 ps, which generally agreed well with performance specification of our light source ($\sim$30 ps) and multichannel PMT ($\sim$150 ps).

2.2. Modulation of the instrument TIRF

We used a fiber dispersion method similar to that described by Ntziachristos *et al* (1998) and Liebert *et al* (2003) to modulate the TIRF of our system. As shown in figure 1, this was achieved by varying the length of the multimode optical fibers on the source and detector sides. The intermodal dispersion properties of the fibers temporally broadened transmitted light pulses with the amount of dispersion directly proportional to fiber length. To ensure as complete modal filling as possible (and therefore to maximize this effect) we placed a diffusing glass plate in front of the source fiber. The overall TIRF of the instrument was then altered by using either (i) a source fiber length (SFL) of 1, 5, 10, or 20 m, with a constant detector fiber length (DFL) of 1 m, (ii) a DFL of 1, 5, 10, or 20 m, with a constant SFL of 1 m, and (iii) SFL and DFL of equal lengths between 1 and 20 m. The rationale here was that we

were interested in separating the effects of either a slower source or detector on the measured instrument PDSF at early time points. Instrument TIRFs for each combination were determined by measuring the temporal transmitted light through a non-scattering water-filled chamber. For these measurements, the source intensity was attenuated by placing ND filters in front of the source fiber to avoid saturation of the PMT array. A thin scattering layer (i.e. a piece of white paper) was placed in front of the detector fiber to ensure complete mode filling, although this was removed for subsequent experiments (section 2.3) where an intralipid solution was used and performed a similar mode-filling function. We determined experimentally (as have other authors) that pulse broadening increased more than twice with the scattering layer in place than with a bare fiber. For our data analysis, equal pulse dispersion was assumed when either the paper or intralipid was in place. As we demonstrate, this fiber dispersion approach allowed broadening of the overall instrument TIRF FWHM from 163 to 716 ps.

2.3. Experimental measurement of the instrument PDSF

To measure the PDSFs we used a similar method to our previous work (Valim *et al* 2010) and translated a 10 cm $\times$ 10 cm absorbing sheet with a centered 2 mm $\times$ 50 mm vertical aperture stepwise through the intralipid media (in our previous work, we used an absorbing rod, but the aperture method was empirically found to reduce inter-experimental variability between measurements). The absorbing sheet was made from anodized foil (BKF12, Thorlabs) and was sufficiently large and opaque to absorb photons not passing through the aperture. The slit was translated through the liquid phantom using computer-controlled stepper motor stages (XSlide, Velmex Inc., Bloomfield, NY). A complete set of measurements were carried out by translation of the slit through 121 steps with a step size of 0.25 mm in the lateral direction (for a total of 3 cm), and through 39 steps with a step size of 0.5 mm in the depth direction. The transmitted light was measured with the PMT array at each slit position. The maximum detected photon count rate was $\sim 10^6$ counts s^{-1} when the slit was positioned directly in front of the laser. By moving the slit to an off-axis position, the count rate dropped to approximately 10^4 counts s^{-1}. We verified that no significant temporal shift of the transmitted photon intensity curve was measured over this range of photon count rates for otherwise identical conditions. We also showed numerically that the measured PDSF with a *slit* aperture had the identical FWHM as a *point* aperture at the center plane (data not shown for brevity) but had the benefit of increasing the photon count rate and improving the measurement signal-to-noise ratio (SNR).

To compute the experimental PDSF, the full time curve through the liquid phantom media was first measured without the slit in place for each fiber combination. This temporal transmitted curve was analyzed to find the timing of the peak point and the 5%-, 10%-, 25%-, and 50%-of-peak time points on the early-time range (i.e. rising edge) of the detected signal. The total photon counts at each slit position were summed within a 32 ps time window (two time points) and the PDSF was then computed as follows:

$$\mathrm{PDSF}(x, z, t) = \frac{I(x, z, t)}{I_{\max}(t)}, \tag{1}$$

where $I_{\max}(t)$ is the maximum transmitted intensity at a given time t and $I(x, z, t)$ is the transmitted intensity at position x, z at time t. As a metric of the overall breadth of the instrument PDSF, we considered the FWHM of the PDSF in the middle plane of the chamber (i.e. $z = 1$ cm) where the extent of photon diffusion was greatest. Broadening of the PDSF due to the finite detection area ($\sim$1.5 mm) at the exit plane of the chamber was minimal in the middle of the chamber. For all experiments, the acquisition time was 1 s per slit position. Each experiment was repeated at least three times for each source and DFL combination. The PDSF FWHM was measured for each experiment individually, and the mean and standard deviation

of all trials at each time point were calculated using standard formulae assuming normally distributed data.

2.4. TR MC simulations

Theoretical PDSFs were computed with a TR MC simulation based on the publically available MCML code on the Oregon Medical Laser Center website (Wang *et al* 1995). MC is a gold standard method for modeling TR photon propagation—particularly at early times where the diffusion approximation to the Boltzmann transport equation (BTE) has been shown to be inaccurate—and is considered a numerical implementation of the BTE. We compiled the paths of photons from a pulsed (infinitely short) pencil beam emerging from a 2 cm semi-infinite slab media at a 1 mm by 1 mm square detector located directly opposite from the input position. The scattering coefficient μ_s was assumed to be 66.7 cm^{-1} based on our reduced scattering coefficient ($\mu\prime_s$) and literature values for the anisotropy coefficient of intralipid at 670 nm, $g = 0.85$ (Flock *et al* 1992). The absorption coefficient was assumed to be $\mu_a = 0.15$ cm^{-1}. A total of 1 billion photons were tracked and the simulation yielded a temporal resolution of 30 ps.

Since TR MC simulations characterize photon propagation through the media for an infinitely short incident pulse, it was also possible to calculate the effect of finite instrument TIRFs on the measured signal using a point-by-point temporal convolution as follows:

$$\text{Measured } (r, z, t) = \int_{-\infty}^{+\infty} \text{MC}(r, z, t - \tau)\text{TIRF}(\tau)\, \mathrm{d}\tau, \tag{2}$$

where $\text{MC}(r, z, t)$ is the photon density at position r and z at time t obtained from the MC simulation respectively, and τ is an integrating factor for time. Here $\text{TIRF}(t)$ was first explicitly measured with our instrument for each of the SFL and DFL combinations as above.

3. Results

3.1. Varying the system TIRF with multimode optical fibers

We first used the multimode fiber pulse dispersion method to vary the overall system TIRF as described. Other authors have shown previously that the degree of pulse dispersion obtained with this method is highly dependent on complete modal filling of the multimode optical fiber (Liebert *et al* 2003). Therefore, for these measurements we placed a thin scattering material (white paper) in front of the detection fiber to mimic the intralipid media. Figure 2(a) shows the broadening effect observed by increasing the source and DFL (in this case, when the SFL and DFL were equal and were increased from 1 to 20 m) on the measured system TIRFs. We quantified this effect by measuring the TIRF FWHM when the fiber length was altered from 1 to 20 m on the source, detector, and source and detector sides as summarized in figures 2(b)–(d), respectively. As shown, increasing the fiber length increased the system TIRF by 5.6 ps m^{-1} on the source side, 11.6 ps m^{-1} on the detector side, and 14.5 ps m^{-1} when both the source and DFL were increased equally. The longest TIRF FWHM we could produce with our method was 716 ps (for SFL = DFL = 20 m), which is on the upper end of instrument TIRF FWHMs reported in the TR literature. The difference in dispersion observed on the source and detector sides was most likely due to sub-optimal mode filling on the source side; it was found that placing a white paper diffuser (versus the glass diffuser) resulted in a further ~50% increase in the TIRF (although paper was not used in the experiments here since it resulted in excessive light loss through the system). Our results indicate less temporal dispersion than reported by Liebert *et al* (2003) that was achieved using a similar method, although we attribute this

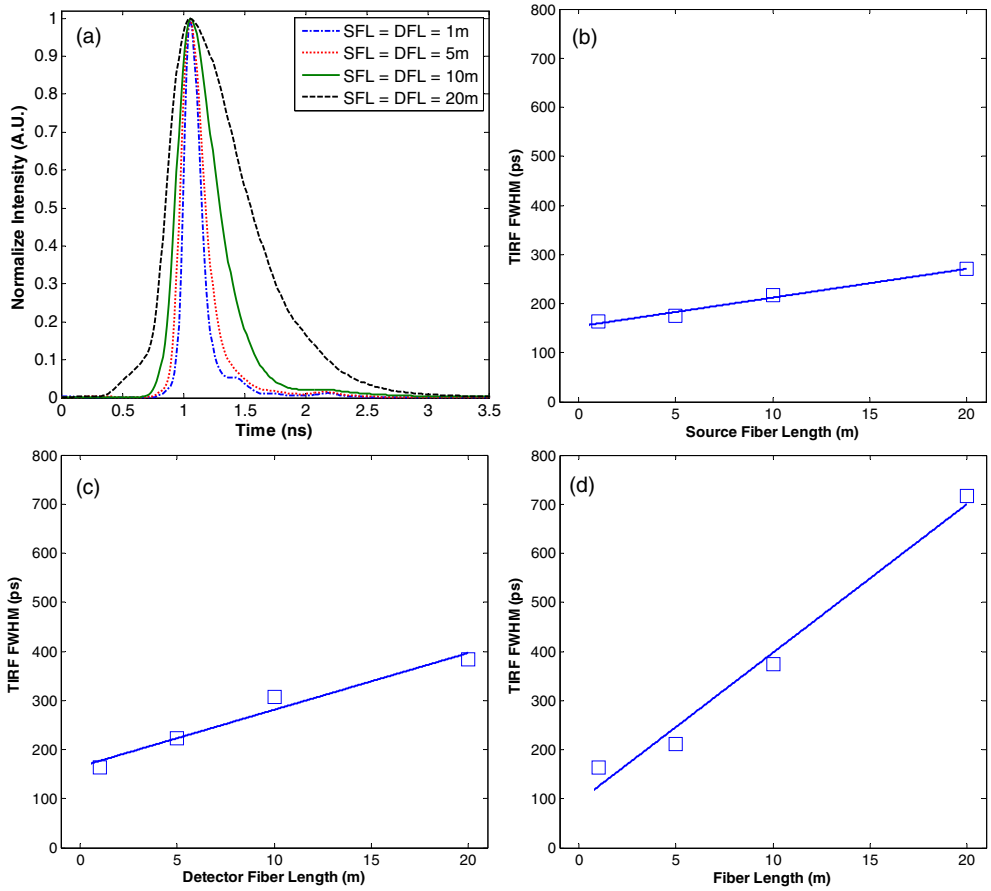

Figure 2. (a) Measured system TIRFs for 1, 5, 10, and 20 m source and DFL. The effect of fiber length from 1 to 20 m on system TIRF FWHM for varying (b) SFL, (c) DFL, and (d) SFL and DFL.

difference to the lower numerical aperture of our fiber, specifically 0.37 versus 0.54. This effect can be estimated using the group delay relationship

$$\frac{\Delta t}{L} = \frac{n}{c_0}\left(\frac{1}{\sqrt{1-\frac{\mathrm{NA}^2}{n^2}}} - 1\right), \tag{3}$$

where c_0 is the speed of light in vacuum, n is the refractive index of the core material, NA the numerical aperture of the fiber, L the length of fiber, and Δt is the delay of the highest order mode in comparison with the lowest order mode. Based on this relationship, use of an NA of 0.54 would have yielded about 2.25 times more dispersion for a fiber of identical length and core index of refraction, consistent with the observed differences. In summary, we verified that it was possible to use this approach to adjust the instrument TIRF without altering major system components (i.e. light sources and detectors).

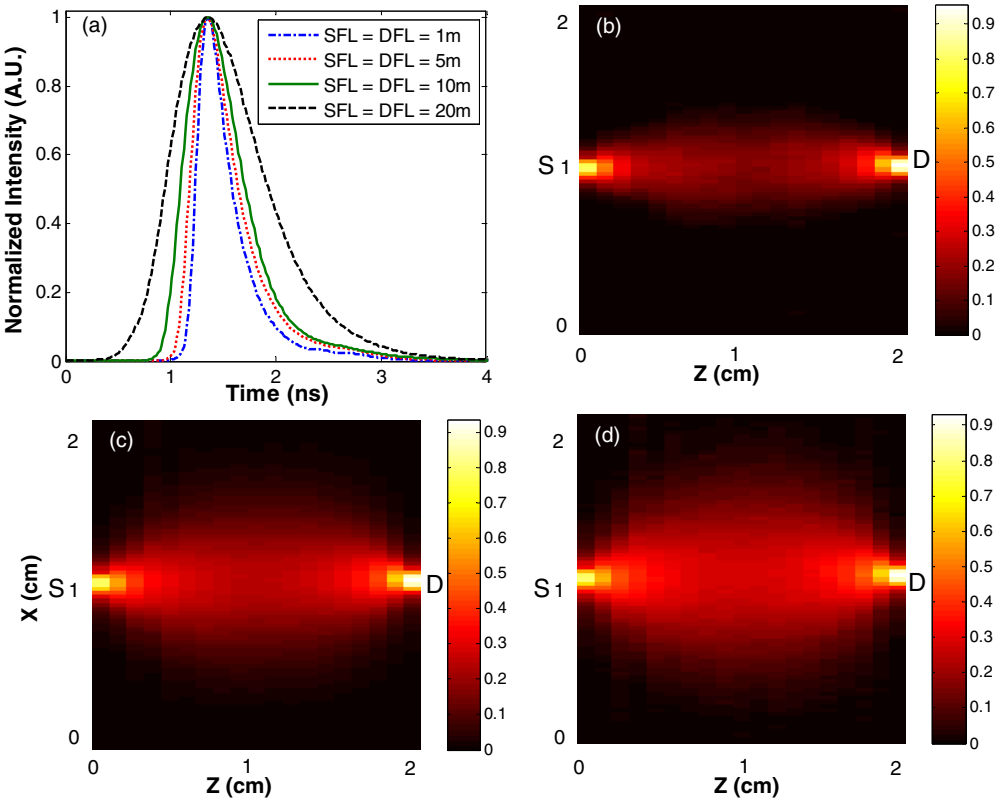

Figure 3. (a) Example measured diffusely transmitted light through the liquid phantom for 1, 5, 10, and 20 m source and DFL. Example measured PDSF for 1 m source and DFL (b) at the 50% point on the rising edge of the TR transmitted curve, (c) quasi-CW photons, and (d) at the 50% point on the falling edge.

3.2. Measurement of instrument PDSFs

We then investigated the effect of the altered TIRF on experimentally measured time-dependent instrument PDSFs. We first filled our 2 cm wide sample chamber with a tissue mimicking intralipid solution and measured the TR transmitted light through the media. As expected, increasing the length of the source and detector fibers (and therefore the instrument TIRF) resulted in significant broadening of the TR transmitted curve. Example curves are shown in figure 3(a) when the source and DFL were equally increased from 1 m (TIRF FWHM = 163 ps) to 20 m (TIRF FWHM = 716 ps). Here, curves were normalized to their maxima, both in amplitude and in time. Temporal normalization to the peak was performed since the true starting point is difficult to accurately measure in practice.

We then translated a rectangular slit aperture through the media and measured the effect on the transmitted curve for each position as described in equation (1). Figures 3(b)–(d) show example PDSFs for the 50% time point on the rising edge, quasi-CW photons, and the 50% time point on the falling edge of the TR curve, respectively, obtained for the fiber configuration corresponding to SFL = DFL = 1 m.

It is evident from the figures that the increase in photon scatter with time resulted in broadening of the measured instrument PDSFs. As expected, time points later than the

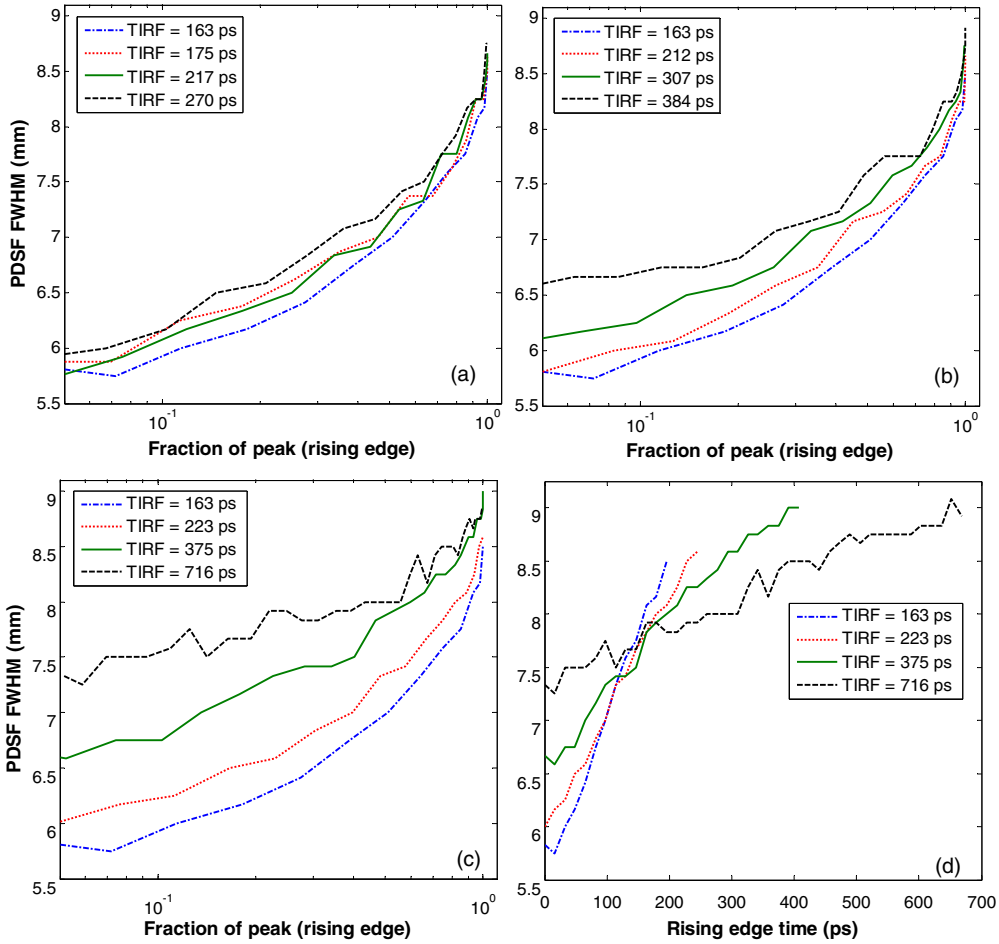

Figure 4. The FWHM of the middle plane of the PDSF at early time points (fraction of the peak point) for varying (a) SFL, (b) DFL, and (c) SFL and DFL. (d) The FWHM of the middle plane of the PDSF versus the measured rise time for varying SFL and DFL.

meantime of the TR curve have PDSFs which are broader than the time-integrated, continuous wave case. For all configurations, we maintained identical photon count rate, laser power, detector gain, and acquisition time to eliminate the possibility of artifacts due to these effects, although this resulted in relatively minor differences in peak transmitted intensities in the TR curve for different TIRFs as discussed below.

We repeated these measurements for all of the SFL and DFL combinations as shown in figure 4 and measured the FWHM of the PDSF in the middle plane of the sample chamber as shown. Since we were principally interested in the use of this approach to improve tomographic imaging resolution, we considered the PDSF FWHM on the 'early' rising edge of the measured TR transmitted curve, i.e. where PDSFs were *narrower* than the un-gated CW case. Measured PDSF FWHM are shown in figures 4(a)–(c) as a function of fraction of peak (i.e. position on the rising edge of the TR curve) for the case where the SFL (figure 4(a)), DFL (figure 4(b)), and both SFL and DFL (figure 4(c)) were varied. Error bars are not shown on plots for clarity, but the measured FWHMs had uncertainty of less than ± 0.25 mm throughout the rising edge of the curve ($N = 3$ for all cases).

As shown, the PDSF breadth increased significantly with longer instrument TIRFs, and the most significant broadening was observed to occur at very early times. Considering the fiber configuration with the fastest TIRF (SFL = DFL = 1 m; TIRF FWHM = 163 ps), the PDSF FWHM at the 10%-of-peak point on the curve was 5.8 ± 0.25 mm compared to the quasi-CW width of 10.5 mm. This represents a relative reduction by about 44.7%, which agrees with our previous results of 40% to 60% over a wide range of conditions (Valim *et al* 2010). In contrast, for the slowest overall TIRF (SFL = DFL = 20 m; TIRF FWHM = 716 ps), the PDSF FWHM at the 10%-of-peak point on the curve was about 7.6 ± 0.1 mm, which is equivalent to a relative reduction of only about 27.6%. For all fiber combinations, when considering the 10%-of-peak point on the transmitted curve, PDSFs broadened in the mid-plane by 0.2 ± 0.1 mm per 100 ps, 0.36 ± 0.06 mm per 100 ps, and 0.29 ± 0.03 mm per 100 ps when the SFL, DFL, and both the SFL and DFL were varied, respectively. Similarly, when considering the 50%-of-peak point on the transmitted curve, the PDSFs broadened by 0.2 ± 0.1 mm per 100 ps, 0.24 ± 0.03 mm per 100 ps, and 0.16 ± 0.07 mm per 100 ps when varying the SFL, DFL, and both the SFL and DFL, respectively. Therefore, our experimental data imply that altering the system TIRF by altering either the source or detector response (or both) results in approximately equivalent effect on the instrument PDSF breadth. We discuss the implications of this below. In the tomographic image reconstruction problem, this PDSF broadening due to the instrument TIRF would directly result in loss of imaging resolution.

For figures 4(a)–(c), we chose to use the 'fraction of peak' as the *x*-axis, as opposed to the *absolute photon arrival time*. The rationale was that these represent points on the measured TR curve with approximately equivalent SNRs, which, in practice, are most relevant for comparison of different instrument configurations. (It is noted that the peak value on the TR curve was slightly less for configurations with longer TIRFs, but that this effect was minimal. Between all configurations studied here the SNR of the peak varied by 3 dB or less.) However, we note that the 10%-of-peak point on the TR curve is actually 'later' on a slower system than the equivalent point on a faster system, since the rise portion of the curve is broadened. We therefore re-plotted the data from figure 4(c) on an absolute time scale in figure 4(d). As shown, PDSF broadening was still observed with the slower configurations (TIRF FWHM = 716 ps) relative to the faster configurations (TIRF FWHM = 163 ps). For example, PDSFs measured in the first 50 ps were broadened by about 1.5 mm or 25%. Here, time curves were aligned at the 0.1%-of-peak point; experimentally, this represents a 'very-early' point on the rising edge of the curve which was about 50 photon counts above background (assuming 5×10^4 photon count peak intensity). In principle, the very earliest points on the 716 ps curve should have PDSF widths that are equivalent to the fastest configuration, but in practice these time points have extremely low SNRs (or are below the system noise floor). Therefore, measurement of even the earliest detectable photons on the TR transmitted curve with the slower system would result in significant loss of tomographic imaging resolution at *any* early time point.

3.3. MC analysis of TR instrument PDSFs

We then considered the effect of the system TIRF on instrument PDSFs computed with TR MC simulations. To consider the effect of finite system TIRFs, we performed point-by-point convolutions of the MC-computed PDSFs (due to an infinitely short laser pulse) with experimentally measured instrument TIRFs. Example results are shown in figure 5(a) for the original output of the MC simulation, as well as convolutions with measured system TIRF FWHM of 163, 223, 375, and 716 ps (corresponding to source and DFL of 1, 5, 10, and 20 m, respectively). In this figure the PDSF FWHM as a function of position on the rising edge of the TR curve is shown for each case. As indicated, the results of the MC simulations were

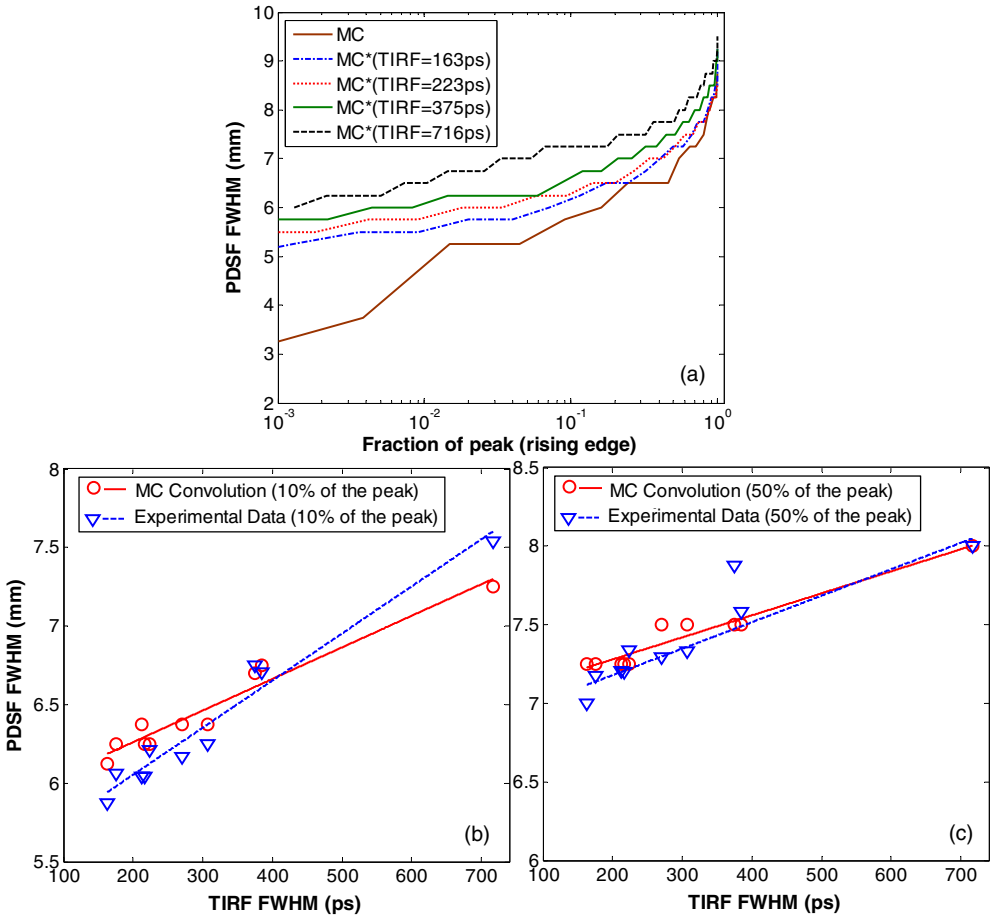

Figure 5. (a) Convolution of the output of TR MC simulations with experimentally measured instrument TIRFs at different points on the rising edge of the transmitted curve. The effects of the TIRF on broadening of the instrument PDSF at the middle plane of the imaging chamber are shown for MC calculations, and experimental measurements at the (b) 10% and (c) 50% of maximum on the rising edge of the TR curve.

qualitatively similar to our experimental results shown in figure 4(c), with the PDSF FWHM increasing in width with increasing instrument TIRFs. For example, at the 10%-of-peak point on the rising edge of the TR curve, the TR MC simulation predicted a PDSF FWHM of 5.75 mm, representing a 45.2% relative reduction in width versus the un-gated CW case. When non-ideal system TIRFs were considered, this resulted in PDSF FWHM broadening up to 7.25 mm (for TIRF FWHM = 716 ps). Earlier time points resulted in even greater relative broadening; for example, at the 0.1%-of-peak point, the PDSF FWHM broadened from 3.25 mm (MC) to 6 mm (for TIRF FWHM = 716 ps).

Overall, TR MC computations yielded 0.2 $\pm$ 0.02 mm per 100 ps broadening of the PDSF FWHM for the 10%-of-peak point, and a 0.15 $\pm$ 0.01 mm per 100 ps broadening for the 50%-of-peak point as shown in figures 5(b) and (c). Generally this analysis agrees well with our experimental data (plotted on the same figures for clarity) where an average of 0.3 $\pm$ 0.02 and 0.17 $\pm$ 0.03 mm per 100 ps broadening of the PDSF FWHM was observed for the

10%- and 50%-of-peak points, respectively. We extrapolated the experimental best-fit curves in figures 5(b) and (c) to the respective *y*-axes (corresponding to infinitely short TIRFs) and obtained 5.45 $\pm$ 0.08 and 6.8 $\pm$ 0.1 mm for the 10%- and 50%-of-peak points, respectively. This was in good agreement with our original MC results (also corresponding to infinitely short TIRFs), of 5.75 and 6.75 mm for the two points. The slight discrepancy in the slope of the 10%-of-peak curves may have been due to minor mismatch between the optical properties of our liquid phantoms and those used in the MC theory, or due to a slight mismatch in the measured system TIRFs with a white paper versus that with intralipid in place.

4. Discussion and conclusions

In recent years, there has been significant renewed interest in the fields of DOT and FMT in the measurement of early-arriving photons to improve imaging resolution, partially driven by the development of new, high speed light sources and detectors (Turner *et al* 2005, Leblond *et al* 2009, Valim *et al* 2010, Venugopal *et al* 2010b, Zhang *et al* 2011, LaPointe *et al* 2012). Our previous work indicated that a reduction in the relative instrument PDSF width by approximately a factor of 2 could be realized over a wide range of conditions by measuring photons that arrived at the 10%-of-peak point on the TR transmitted curve using our supercontinuum laser and PMT combination (Valim *et al* 2010). It was also determined that further reduction in the PDSF width could *not* be obtained at *earlier* time points (<10%-of-peak), even though MC simulations predicted that a reduction of 3–4 times should be obtainable. In other words, we experimentally observed a 'leveling out' of the early-photon effect that was not predicted by theory. As such, the experiments described in this work were performed to quantify the relationship between system TIRF and time-dependent instrument PDSF widths over a range of response times that were generally representative of previously reported literature values (from 163 to 716 ps).

Two important conclusions from this work are noted. First, while it is generally understood that 'faster is better' for TR DOT and FMT systems, our data indicate that substantial disagreement was observed versus TR MC models for *all* experimental instrument TIRFs considered. Further, the effect was larger at earlier time points, where up to 19%, 32%, and 40% error were observed at the 50%-, 10%-, and 5%-of-peak points on the transmitted intensity curve, respectively. Experimental and MC analysis showed that this broadening was fairly linear and was 0.15 to 0.3 mm per 100 ps for the system TIRF (depending on the position on the TR curve). As such, these results confirm that the 'leveling out' of the early-photon effect observed in our previous work was most likely due to the non-ideal system TIRF. Although systems with longer TIRFs resulted in temporally extending the rise portion of the transmitted intensity curve, in practice *all* usable points—in this case all points on the rising portion on the TR transmitted curve above 0.1% of the peak value—yielded broadened PDSFs versus faster systems. In a DOT or FMT imaging system, this would yield a corresponding loss in imaging resolution. Likewise, significantly narrower PDSFs and improved imaging resolution should be obtainable with faster systems, although this was not explicitly confirmed here. However, it is critical to re-iterate that the imaging resolution obtained in DOT and FMT is not only a function of the instrument PDSF width, but also the noise and sensitivity properties of the measurements, i.e. two systems with identical TIRF but disparate SNRs will yield different overall imaging performance.

Second, our data indicate that PDSF broadening was approximately equal when the instrument TIRF was increased on either the source or detector sides (or both simultaneously). In terms of the design of TR DOT or FMT systems, this implies that no particular advantage would be obtained by using a faster pulsed laser or detector, so that the net effect on the overall

system TIRF should be considered (again, this neglects effects of detector sensitivity and noise performance in the DOT inverse problem). As noted in the introduction, several groups have attempted to measure early photons with a range of detector types, including MCPs, PMTs, ICCDs, streak cameras, and fast APDs. One evident issue therefore is the generalizability of these results for systems with alternate component types. For example we cannot rule out the possibility that two detectors with identical TIRFs but with different sensitivity and noise properties would yield different instrument PDSF widths. However, the results of our studies with TR MC data generally agree very well with our experimental data, and therefore our data indicate that simple convolution of the instrument TIRF appears to entirely account for the observed PDSF broadening effect. These data also underscore the importance of correcting PDSFs for instrument TIRFs via convolution when performing tomographic image reconstruction to ensure accurate data–model agreement.

Acknowledgments

This work was funded with a grant from the National Institutes of Health (R01EB012117-01) and from a Northeastern University laboratory startup grant.

References

Andersson-Engels S, Berg R, Svanberg S and Jarlman O 1990 Time-resolved transillumination for medical diagnostics *Opt. Lett.* **15** 1179–81

Arridge S R 1999 Optical tomography in medical imaging *Inverse Probl.* **15** R41–93

Bérubé-Lauzière Y and Robichaud V 2007 Time-of-flight non-contact fluorescence diffuse optical tomography with numerical constant fraction discrimination *Proc. SPIE* **6629** 66290Y

Boas D A, Brooks D H, Miller E L, DiMarzio C A, Kilmer M, Gaudette R J and Zhang Q 2001 Imaging the body with diffuse optical tomography *IEEE Signal Process. Mag.* **18** 57–75

Contini D, Torricelli A, Pifferi A, Spinelli L, Paglia F and Cubeddu R 2006 Multi-channel time-resolved system for functional near infrared spectroscopy *Opt. Express* **14** 5418–32

Culver J P, Durduran T, Furuya D, Cheung C, Greenberg J H and Yodh A G 2003 Diffuse optical tomography of cerebral blood flow, oxygenation, and metabolism in rat during focal ischemia *J. Cereb. Blood Flow Metab.* **23** 911–24

Flock S T, Jacques S L, Wilson B C, Star W M and van Gemert M J 1992 Optical properties of Intralipid: a phantom medium for light propagation studies *Lasers Surg. Med.* **12** 510–9

Gandjbakhche A H, Nossal R and Bonner R F 1994 Resolution limits for optical transillumination of abnormalities deeply embedded in tissues *Med. Phys.* **21** 185–91

Gerega A, Zolek N, Soltysinski T, Milej D, Sawosz P, Toczylowska B and Liebert A 2011 Wavelength-resolved measurements of fluorescence lifetime of indocyanine green *J. Biomed. Opt.* **16** 067010

Graves E E, Ripoll J, Weissleder R and Ntziachristos V 2003 A submillimeter resolution fluorescence molecular imaging system for small animal imaging *Med. Phys.* **30** 901–11

Grosenick D, Moesta K T, Wabnitz H, Mucke J, Stroszczynski C, Macdonald R, Schlag P M and Rinneberg H 2003 Time-domain optical mammography: initial clinical results on detection and characterization of breast tumors *Appl. Opt.* **42** 3170–86

Grosenick D, Wabnitz H, Rinneberg H H, Moesta K T and Schlag P M 1999 Development of a time-domain optical mammograph and first *in vivo* applications *Appl. Opt.* **38** 2927–43

Hee M R, Izatt J A, Swanson E A and Fujimoto J G 1993 Femtosecond transillumination tomography in thick tissues *Opt. Lett.* **18** 1107–9

Hielscher A H 2005 Optical tomographic imaging of small animals *Curr. Opin. Biotechnol.* **16** 79–88

Hillman E M C, Hebden J C, Schmidt F E W, Arridge S R, Schweiger M, Dehghani H and Delpy D T 2000 Calibration techniques and datatype extraction for time-resolved optical tomography *Rev. Sci. Instrum.* **71** 3415–27

Kacprzak M, Liebert A, Staszkiewicz W, Gabrusiewicz A, Sawosz P, Madycki G and Maniewski R 2012 Application of a time-resolved optical brain imager for monitoring cerebral oxygenation during carotid surgery *J. Biomed. Opt.* **17** 016002

Kepshire D, Mincu N, Hutchins M, Gruber J, Dehghani H, Hypnarowski J, Leblond F, Khayat M and Pogue B W 2009 A microcomputed tomography guided fluorescence tomography system for small animal molecular imaging *Rev. Sci. Instrum.* **80** 043701

Klose A D, Ntziachristos V and Hielscher A H 2005 The inverse source problem based on the radiative transfer equation in optical molecular imaging *J. Comput. Phys.* **202** 323–45

Kumar A T, Raymond S B, Dunn A K, Bacskai B J and Boas D A 2008 A time domain fluorescence tomography system for small animal imaging *IEEE Trans. Med. Imaging* **27** 1152–63

LaPointe E, Pichette J and Berube-Lauziere Y 2012 A multi-view time-domain non-contact diffuse optical tomography scanner with dual wavelength detection for intrinsic and fluorescence small animal imaging *Rev. Sci. Instrum.* **83** 063703

Leblond F, Dehghani H, Kepshire D and Pogue B W 2009 Early-photon fluorescence tomography: spatial resolution improvements and noise stability considerations *J. Opt. Soc. Am. A Opt. Image Sci. Vis.* **26** 1444–57

Li L and Wang L H V 2007 Optical coherence computed tomography *Appl. Phys. Lett.* **91** 141107

Liebert A, Wabnitz H, Grosenick D and Macdonald R 2003 Fiber dispersion in time domain measurements compromising the accuracy of determination of optical properties of strongly scattering media *J. Biomed. Opt.* **8** 512–6

Liebert A, Wabnitz H, Steinbrink J, Obrig H, Moller M, Macdonald R, Villringer A and Rinneberg H 2004 Time-resolved multidistance near-infrared spectroscopy of the adult head: intracerebral and extracerebral absorption changes from moments of distribution of times of flight of photons *Appl. Opt.* **43** 3037–47

Luchowski R, Gryczynski Z, Sarkar P, Borejdo J, Szabelski M, Kapusta P and Gryczynski I 2009 Instrument response standard in time-resolved fluorescence *Rev. Sci. Instrum.* **80** 033109

Niedre M and Ntziachristos V 2010 Comparison of fluorescence tomographic imaging in mice with early-arriving and quasi-continuous-wave photons *Opt. Lett.* **35** 369–71

Niedre M J, Turner G M and Ntziachristos V 2006 Time-resolved imaging of optical coefficients through murine chest cavities *J. Biomed. Opt.* **11** 064017

Ntziachristos V, Bremer C and Weissleder R 2003 Fluorescence imaging with near-infrared light: new technological advances that enable *in vivo* molecular imaging *Eur. Radiol.* **13** 195–208

Ntziachristos V and Chance B 2001 Accuracy limits in the determination of absolute optical properties using time-resolved NIR spectroscopy *Med. Phys.* **28** 1115–24

Ntziachristos V, Ma X H and Chance B 1998 Time-correlated single photon counting imager for simultaneous magnetic resonance and near-infrared mammography *Rev. Sci. Instrum.* **69** 4221–33

Ntziachristos V, Ripoll J, Wang L V and Weissleder R 2005 Looking and listening to light: the evolution of whole-body photonic imaging *Nature Biotechnol.* **23** 313–20

Ntziachristos V, Yodh A G, Schnall M and Chance B 2000 Concurrent MRI and diffuse optical tomography of breast after indocyanine green enhancement *Proc. Natl Acad. Sci. USA* **97** 2767–72

Pifferi A, Swartling J, Chikoidze E, Torricelli A, Taroni P, Bassi A, Andersson-Engels S and Cubeddu R 2004 Spectroscopic time-resolved diffuse reflectance and transmittance measurements of the female breast at different interfiber distances *J. Biomed. Opt.* **9** 1143–51

Sawosz P, Kacprzak M, Zolek N, Weigl W, Wojtkiewicz S, Maniewski R and Liebert A 2010 Optical system based on time-gated, intensified charge-coupled device camera for brain imaging studies *J. Biomed. Opt.* **15** 066025

Torricelli A, Pifferi A, Taroni P, Giambattistelli E and Cubeddu R 2001 *In vivo* optical characterization of human tissues from 610 to 1010 nm by time-resolved reflectance spectroscopy *Phys. Med. Biol.* **46** 2227–37

Tosi A, Dalla Mora A, Zappa F, Gulinatti A, Contini D, Pifferi A, Spinelli L, Torricelli A and Cubeddu R 2011 Fast-gated single-photon counting technique widens dynamic range and speeds up acquisition time in time-resolved measurements *Opt. Express* **19** 10735–46

Tromberg B J, Coquoz O, Fishkin J B, Pham T, Anderson E R, Butler J, Cahn M, Gross J D, Venugopalan V and Pham D 1997 Non-invasive measurements of breast tissue optical properties using frequency-domain photon migration *Phil. Trans. R. Soc. B Biol. Sci.* **352** 661–8

Turner G M, Zacharakis G, Soubret A, Ripoll J and Ntziachristos V 2005 Complete-angle projection diffuse optical tomography by use of early photons *Opt. Lett.* **30** 409–11

Valim N, Brock J and Niedre M 2010 Experimental measurement of time-dependent photon scatter for diffuse optical tomography *J. Biomed. Opt.* **15** 065006

Venugopal V, Chen J and Intes X 2010a Development of an optical imaging platform for functional imaging of small animals using wide-field excitation *Biomed. Opt. Express* **1** 143–56

Venugopal V, Chen J, Lesage F and Intes X 2010b Full-field time-resolved fluorescence tomography of small animals *Opt. Lett.* **35** 3189–91

Wabnitz H, Moeller M, Liebert A, Obrig H, Steinbrink J and Macdonald R 2010 Time-resolved near-infrared spectroscopy and imaging of the adult human brain *Adv. Exp. Med. Biol.* **662** 143–8

Wang L, Jacques S L and Zheng L 1995 MCML–Monte Carlo modeling of light transport in multi-layered tissues *Comput. Methods Programs Biomed.* **47** 131–46

Wang L V and Wu H-i 2007 *Biomedical Optics: Principles and Imaging* (Hoboken, NJ: Wiley-Interscience)

Wu J, Perelman L, Dasari R R and Feld M S 1997 Fluorescence tomographic imaging in turbid media using early-arriving photons and Laplace transforms *Proc. Natl Acad. Sci. USA* **94** 8783–8

Zhang B, Cao X, Liu F, Liu X, Wang X and Bai J 2011 Early-photon fluorescence tomography of a heterogeneous mouse model with the telegraph equation *Appl. Opt.* **50** 5397–407

Zhao Q, Spinelli L, Bassi A, Valentini G, Contini D, Torricelli A, Cubeddu R, Zaccanti G, Martelli F and Pifferi A 2011 Functional tomography using a time-gated ICCD camera *Biomed. Opt. Express* **2** 705–16